Available online at www.sciencedirect.com
SCIENCE DIRECT®
Mechanics of Materials 36 (2004) 601–622
MECHANICS OF MATERIALS
www.elsevier.com/locate/mechmat

Simulations of crack propagation in elastic–plastic graded materials

Zhiqiang Wang, Toshio Nakamura *

Department of Mechanical Engineering, State University of New York at Stony Brook, Stony Brook, NY 11794, USA

Received 19 November 2002; received in revised form 20 May 2003

Abstract

This paper introduces a criterion suitable for the simulation of crack propagation in elastic–plastic graded materials. It proposes a power-law relationship between the two critical failure parameters, surface separation energy and peak separation stress, which are spatial variants in graded solids. To investigate its feasibility, this criterion is implemented in finite element models and tested under various dynamic failure conditions. First, dynamic crack propagation in double cantilever beam model is considered and the effects of the failure parameters are investigated. The results show crack propagation behavior is highly dependent on the variations of the failure parameters. Evolutions of various energy components are also monitored during the crack growth to evaluate failure characteristics of graded materials. Unlike homogeneous materials, crack propagation in elastic–plastic graded materials never attains a steady state and the fracture energy associated with crack growth continues to vary as the crack propagates through the graded region. In a subsequent analysis, impact failure of a ceramic–metal graded layer is considered. In this case, multiple crack initiate and propagate at various locations. Additionally, different through-thickness compositional gradations are examined to study their effects on cracking profiles and energy absorption characteristics. It is demonstrated that the cracking substantially alters the overall pattern of energy evolutions even though the energy directly consumed by the surface separations remains small. This study concludes that similar approaches can be employed for investigating failure in other inhomogeneous/heterogeneous materials to optimize their design.

Keywords: Crack propagation; Graded materials; FGM; Fracture energy; Separation energy; Cohesive model

1. Introduction

Graded materials or functionally graded materials (FGMs) are being increasingly considered for various applications to maximize the strength and integrity of engineering components. In a graded material, the distribution of multiple phases is spatially varied within the body, which allows for the optimization of the material compositions, and their the effective properties for a given application. Potential applications include materials that are resistant to dynamic loads and high temperatures (e.g. Chin, 1999; Suresh, 2001). However, crack propagation in graded materials is an inherently complex phenomena, because of spatial variations

* Corresponding author. Tel.: +1-631-632-8312; fax: +1-631-632-8544.
E-mail address: toshio.nakamura@sunysb.edu (T. Nakamura).

0167-6636/$ - see front matter © 2003 Elsevier Ltd. All rights reserved.
doi:10.1016/S0167-6636(03)00079-6

in fracture properties. As a result, crack growth criteria applicable for graded materials must be able to accommodate non-uniformity in fracture toughness, which severely limits the applicability of conventional models developed for fracture simulation studies in homogeneous materials.

Fracture behavior of FGMs has been the subject of a number of earlier investigations. For a metal–ceramic graded materials, an increasing fracture toughness was observed when the crack propagated from a ceramic rich region to a metal rich region (Jin and Batra, 1996; Cai and Bao, 1998; Li et al., 2000). An experimental investigation of dynamic fracture of such materials, conducted by Parameswaran and Shukla (1998), demonstrated that the crack advance distance decreases with increasing toughness. Marur and Tippur (2000) showed that the Mode II stress intensity factor is strongly influenced by the material gradient and crack position due to strong dependence on sliding displacements of the crack flanks. The influence of elastic gradient profile was also investigated by Rousseau and Tippur (2001, 2002), who suggested that the elastic gradient profile had a larger effect when crack resided on the compliant side rather than on the stiffer side. Their analysis also evaluated crack tip fields and stress intensity factors for cracks parallel to the elastic gradient in FGMs. Becker et al. (2002) used Weibull statistics for the predictions of crack toughness and average initiation angle in brittle FGMs, and evaluated the fracture behavior for various gradients. Several analytical studies have also been conducted to investigate the fracture behavior of graded materials. Konda and Erdogan (1994) studied singular crack tip stress field in graded materials, and Konda and Erdogan (1994) used the conservation integral to determine the J-integral. An energy-based model was studied by Kolednik and Suresh (1999) to quantify the influence of the plasticity gradient on the fracture resistance. However, it should be noted that most of these analyses assumed either stationary cracks or linear elastic behavior.

The current analysis focuses on crack propagation in elastic–plastic graded materials. While this problem has been well studied for the case of homogeneous solids, investigations for inhomogeneous materials, such as graded materials, are limited. Thus, our objective is to establish a proper fracture simulation procedure that would be applicable for understanding the failure behavior of graded materials. Furthermore, since it is difficult to perform accurate and meaningful fracture experiments on FGMs, a simulation studies will provide valuable insights towards characterizing these materials. As an example, Fig. 1 shows a fracture test conducted on a graded material. Here the specimen was fabricated using the plasma sprayed technique where the volume fractions of partially-stabilized zirconia (PSZ) and NiCrAlY are gradually varied. A notched fracture specimen fabricated from this material was then subjected to

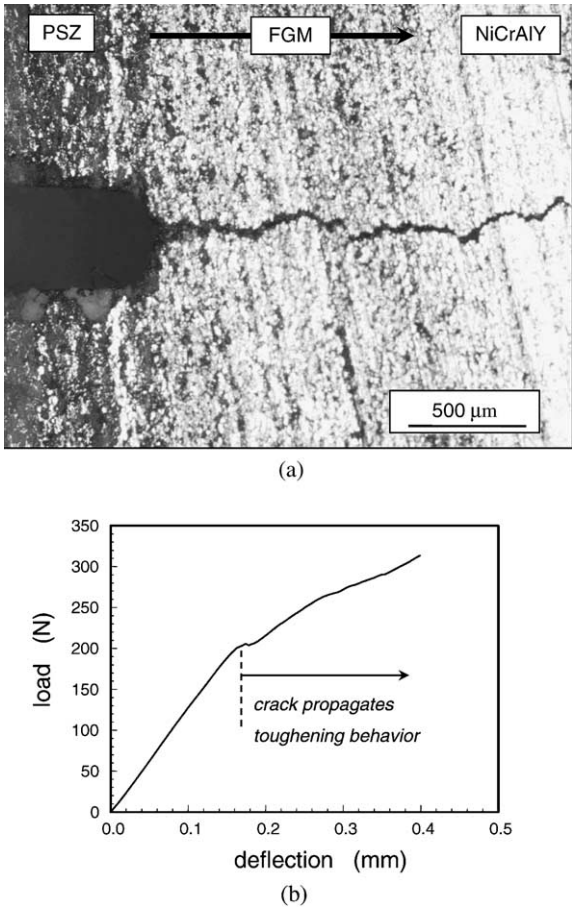

Fig. 1. (a) Fractured elastic–plastic graded specimen under three-point-bend load. (b) Load–displacement record of preliminary test, which indicates increasing toughness as crack propagates into tougher phase.

three-point-bending, and a crack was observed to propagate from the brittle PSZ phase to the more ductile NiCrAlY phase. Even though some measurements are made as shown in the figure, given the small size of the specimen, quantitative interpretation of test data evaluations was difficult. Thus one has to relay on a simulation study to characterize the failure mechanisms. Note that simulations of propagation require the knowledge of variations in compositions, material and other properties in the graded region.

Prior to performing a simulation study, it is necessary to establish a fracture model that can accommodate non-uniform fracture condition since graded materials exhibit location dependent fracture responses. First, a new criterion is proposed. Then, the feasibility of the model is examined in a dynamic fracture analysis of double cantilever beam (DCB) specimen. Subsequently, the proposed fracture criterion is implemented in a more complex model. Here a ceramic–metal graded protective layer is impacted by a high-velocity rod which causes multiple crack initiations and propagations. The aim is to quantify the influence of material gradation on the fracture as well as the energy absorption behaviors. This analysis provides a computational tool necessary to optimize material gradation to meet its design requirements.

2. Crack propagation in graded materials

2.1. Fracture model based on energy concept

The Griffith criterion for crack growth in an ideally brittle elastic solid is given as,

$$\Gamma = \Gamma_o. \tag{1}$$

Here Γ_o is the material's surface separation/fracture energy per unit area, and Γ is the energy release rate required for the crack advance. For 2-D dynamic crack propagation (along x-direction) in elastic media, Γ can be computed via the domain integral as,

$$\Gamma = \int_A [\sigma_{ij}u_{i,j}q_{,j} - (W+K)q_{,1} + \rho(\ddot{u}_i u_{i,1} - \dot{u}_i \dot{u}_{i,1})q]\,\mathrm{d}A. \tag{2}$$

Here, σ_{ij} and u_i are the Cartesian components of stress and displacement, W and K are the strain and kinetic energy densities, respectively, A is the area of a domain includes the crack tip, and $(\dot{})$ denotes time derivative. The weighting function q has the value of unity at the tip and zero at the boundary of the domain. The above integral has been used successfully in computing energy release rate of dynamically propagating cracks (e.g., Nakamura et al., 1986).

For elastic–plastic materials, the total energy required to propagate a crack also includes the energy dissipation through formation of near tip plastic zone. The total energy due to fracture, therefore, can be expressed as (Tvergaard and Hutchinson, 1992),

$$\Gamma = \Gamma_o + \Gamma_p. \tag{3}$$

Here Γ_p is the plastic dissipation energy due to unit crack advance. Since Γ_p is controlled by the near tip constraint and loading conditions, the total work of fracture is not a material constant. In general, Γ_o may be assumed as a constant while Γ_p varies as crack propagates except under steady-state condition. For *inhomogeneous* materials, both Γ_o and Γ_p should be functions of spatial coordinates. Suppose material properties vary continuously along the x-direction, the total work of fracture in the graded materials can be expressed as,

$$\Gamma(x) = \Gamma_o(x) + \Gamma_p(x). \tag{4}$$

Here the surface separation energy $\Gamma_o(x)$ may be treated as a spatially variant material parameter while the plastic dissipation $\Gamma_p(x)$ is a geometry dependent parameter. Again, the total work of fracture $\Gamma(x)$ is not a material parameter since it depends on the loading and boundary conditions.

The energy flow into a moving crack tip can be also expressed via the equation of energy rate balance. If crack propagates within an elastic body, it is given as,

$$F = P - (\dot{U}_{el} + \dot{T}). \tag{5}$$

Here F is the rate of total energy dissipated out of the body, P is the power of external load, U_{el} is the total *elastic* strain energy and T is the total kinetic

energy. When the crack propagates at speed v, the energy release rate is $\Gamma = F/v$ and equivalent to the integral shown in (2). For elastic–plastic media, the energy required to separate crack surfaces can be approximated as,

$$F_o = P - (\dot{U} + \dot{T}). \tag{6}$$

In this equation, U is the total stress work containing both the elastic and plastic parts (e.g., $U = U_{el} + U_{pl}$). The above expression assumes the entire plastic flow within a body to be directly caused by the moving crack. If plastic flow occurs away from the crack tip (e.g., load application point), such dissipation must be subtracted from U_{pl}. Alternatively, one may assume the above equation to hold within a contained region that includes near tip plastic zone but excludes plastic deformation near the loading boundary. With this relation, the separation energy Γ_o and the plastic dissipation Γ_p caused by crack advance are,

$$\Gamma_o = \frac{F_o}{v} \quad \text{and} \quad \Gamma_p = \frac{\dot{U}_{pl}}{v}. \tag{7}$$

In the present elastic–plastic graded materials, the separation energy Γ_o is assumed as a material property that implicitly depends on material composition while Γ_p is treated as the plastic dissipation due to crack advance through the graded region. The latter parameter is usually a strong function of the failure stress required to separate surfaces. In general, he separation energy Γ_o can be dependent on the mode-mixity as well as on the crack tip speed. The mode dependency is examined but the influence of crack tip speed is not considered in this paper to keep the analysis simple.

2.2. Models for crack growth simulation

There are several methods to simulate crack propagation in homogeneous elastic–plastic materials. They have been used to investigate the role of plasticity during the fracture process under various conditions. One of more popular methods utilizes the 'embedded process zone' (EPZ), which incorporates a cohesive or surface traction–separation law to characterize fracturing process (Needleman, 1987; Tvergaard and Hutchinson, 1992, 1996; Tvergaard, 2001). This law is embedded as an internal boundary condition or in special elements along the fracture plane. The parameters governing the separation law are the separation energy Γ_o the peak traction/separation stress σ_{max} and the reference opening displacement of the crack surfaces δ_o. Although there are various traction–displacement relations (e.g., Xu and Needleman, 1994; Camacho and Ortiz, 1996; Geubelle and Baylor, 1998), they may be classified into the EPZ category. Usually, a precise nature of traction–separation relation is not important, and only the magnitudes of Γ_o and σ_{max} directly influence the fracturing process. Because of the plastic yielding, the EPZ model is limited to the cases in which the ratio of σ_{max} to the yield stress σ_o is not too large. Otherwise, stress levels achieved near crack tip are not high enough to produce surface separation. The upper limit of σ_{max}/σ_o is about 3.0 for an elastic–perfectly plastic material (Tvergaard and Hutchinson, 1996). Similar models that incorporate cohesive model have been used for elastic failure analyses under dynamic conditions (e.g., Breitenfeld and Geubelle, 1998; Repetto et al., 2000; Ruiz et al., 2001) and in the micro-mechanical failure analysis of heterogeneous ceramic systems (Zhai and Zhou, 2000). The EPZ approach based on experimental observations was recently discussed by Hutchinson and Evans (2000).

The limitation of the EPZ model motivated the development of the plasticity-free strip or SSV model. Assuming dislocations emitted at the crack tip play a minimal role in crack propagation, Suo, Shih and Varias (SSV) introduced the idea of plasticity-free strip (Suo et al., 1993; Beltz et al., 1996). In the SSV model, an elastic (plasticity-free) layer is imposed between the crack plane and the plastic zone. In this model, there is no explicit recognition of a separation law because the traction on the crack tip is unbounded as the tip is approached. It is assumed that the size of any separation zone should be sufficiently small compared to the thickness of the plasticity-free layer D such that the peak separation stress is always achieved. Therefore, σ_{max} is not a parameter in this model. The criterion for crack propagation is simply $\Gamma_{tip} = \Gamma_o$, where, Γ_{tip} is the energy release rate near the crack tip. In contrast to the EPZ

model, the SSV model becomes invalid at low separation strength because the size of the separation zone becomes comparable to or larger than D. Under such condition, the assumption of attaining the peak separation stress is violated. Since both EPZ and SSV models have some limitations, so-called 'unified model' was developed by Wei and Hutchinson (1999). It incorporates both the traction–separation description used in the EPZ model and the plasticity-free layer of thickness of thickness of D in the SSV model. The crack plane is characterized by the adhesion energy Γ_o and the separation strength σ_{max}, and the thickness of the plasticity-free zone D. When D becomes small, the unified model converges to the EPZ model. When σ_{max} is larger, it approaches the SSV model. Compared with the EPZ and SSV models, the unified model can accommodate larger variations of material parameters.

In addition to these models based on the macroscopic fracture toughness, a model based on the micro-scale failure process was introduced by Xia and Shih (1995). Here near tip void growths and their eventual coalescence are considered. In many ductile materials, most of the separation energy Γ_o is consumed during the void nucleation and coalescence. In Xia and Shih (1995), an element layer of void-containing cells was introduced ahead of crack. The element size is in the same order as the spacing of the inclusions, which can initiate voids. When stress is applied, the void in the cell grows, and the volume fraction of void increases and the cell weakens. Eventually these voids coalesce and the crack advances across the cells to form a longer crack. Instead of defining fracture conditions in special elements or boundary conditions, the virtual internal bond (VIB) model was introduced to incorporate the fracture law directly into the constitutive equations of regular elements (Gao and Klein, 1998; Klein and Gao, 1998). In this approach, cohesive bonds connecting randomly distributed material particles are incorporated within continuum elements. The collective behavior of this random bond network is determined by equating the strain energy function on the continuum level to the potential energy stored in the cohesive bonds in the micro-scale. In this model, the fracture energy is not a constant for a given material. It depends strongly on the deformation conditions near the crack tip. One of the promising features of this model is that it provides a means to combine the plasticity theory with the fracture model at the constitutive level. This method has been applied to simulate crack nucleation and propagation in a ductile layer between two brittle layers, and toughness increasing due to plastic deformation has been observed (Gao and Klein, 1998; Klein and Gao, 1998). The merits and disadvantages of these crack growth models are summarized in Table 1.

In the present work, several factors were considered in selecting a suitable simulation model for graded materials. One is computational effectiveness. Since graded or inhomogeneous materials generally require more computational efforts than those for homogeneous materials, additional

Table 1
Summary of various elastic–plastic failure simulation models

Models	Advantages	Disadvantages
EPZ	Various separation laws can be easily accommodated. Implementation to existing code is simple	Fails to provide predictions when peak separation stress is too high compared with yield stress. Artificial compliance along element boundary may be introduced
SSV	Suitable when separation stress is large	Size of the elastic strip may affect fracture behavior
Unified (EPZ + SSV)	Applicable for various conditions of elastic–plastic crack propagation	More parameters (both separation law and elastic strip) are needed
Cell	Able to simulate void nucleation and coalescence	Calibration from experimental data may be complex
VIB	Separation law is incorporated into the constitutive relation. No artificial compliance is introduced	Difficult to implement and tends to be numerically unstable for inhomogeneous materials. Requires large CPU time

processing needed for a crack growth simulation must be kept at reasonable level. An ease of implementation is also an important consideration in models containing complex materials. This means that the VIB model is not suitable since it requires significant computational time and the numerical convergence is often difficult to achieve. Another requirement is the ability to simulate multiple crack initiations and growths at arbitrary locations. This condition is necessary for cracking under impact load or when crack paths are not known a priori. Of aforementioned models, the SSV, unified and void-containing cell models require prior knowledge of crack paths, and therefore, they are not suitable. Thus, only the EPZ model appears to be eligible for the failure simulations of inhomogeneous materials under general conditions. The actual separation law adopted in our analyses uses the traction–separation relation utilized by Xu and Needleman (1994). Here so-called cohesive elements are inserted along boundaries of continuum elements to simulate surface separation.

2.3. Surface separation model

To achieve separation of crack surfaces along element boundaries, special elements that follow appropriate traction–displacement relation are used. In general, the cohesive element acts as a non-linear spring and the crack growth criterion is embedded in its constitutive equation. The traction–displacement relation of the cohesive element is defined through a potential function Φ. Since the energy required to separate two nodes is equivalent to the integral of traction over displacement, Φ represents the amount of consumed energy due to a growing crack. When crack grows under mixed-mode condition, this potential function includes both the normal (Mode I) and tangential (Mode II) contributions as (Xu and Needleman, 1994),

$$\Phi(\delta^{\mathrm{n}},\delta^{\mathrm{t}}) = \Gamma_{\mathrm{o}}\left\{1+\mathrm{e}^{-\delta^{\mathrm{n}}/\delta^{\mathrm{n}}_{\mathrm{o}}}\left[\left(1+\frac{\delta^{\mathrm{n}}}{\delta^{\mathrm{n}}_{\mathrm{o}}}\right)(q-1) - \left(1+\frac{\delta^{\mathrm{n}}}{\delta^{\mathrm{n}}_{\mathrm{o}}}\right)q\mathrm{e}^{-(\delta^{\mathrm{t}}/\delta^{\mathrm{t}}_{\mathrm{o}})^2}\right]\right\}. \tag{8}$$

Here δ^{n} and δ^{t} are the displacement components normal and tangential to the crack surfaces, respectively. Also $\delta^{\mathrm{n}}_{\mathrm{o}}$ and $\delta^{\mathrm{t}}_{\mathrm{o}}$ are the reference displacements, q is the ratio of the separation energy under pure Mode II and pure Mode I conditions. If $q=1$, equal separation energies are assumed for Modes I and II. The normal and shear traction components can be derived through the partial derivatives of Φ with respect to δ^{n} and δ^{t}, respectively. For the normal component, the peak traction/stress $\sigma_{\max} = \Gamma_{\mathrm{o}}/e\delta^{\mathrm{n}}_{\mathrm{o}}$ occurs at $\delta^{\mathrm{n}} = \delta^{\mathrm{n}}_{\mathrm{o}}$ while the maximum shear traction $\tau_{\max}$ occurs at $\delta^{\mathrm{t}} = \delta^{\mathrm{t}}_{\mathrm{o}}/\sqrt{2}$. The reference tangential displacement is $\delta^{\mathrm{t}}_{\mathrm{o}} = \sqrt{2}e\delta^{\mathrm{n}}_{\mathrm{o}}\sigma_{\max}/\tau_{\max}$. A potential source of error for this type of cohesive separation model is that an artificial *compliance* can be introduced between regular elements. When choosing parameters, this effect must be considered carefully. Under pure Mode I condition, Γ_{o} should be set according the material's separation energy while either $\sigma_{\max}$ or δ_{o} can be set independently. In *linear elastic* materials, choice of $\sigma_{\max}$ or δ_{o} is not very important although it can influence the numerical accuracy. Nakamura and Wang (2001) have reported that for ideally brittle materials, the numerical error decreases with higher values of $\sigma_{\max}$ (i.e., smaller values of δ_{o}). In *elastic–plastic* materials, selection of $\sigma_{\max}$ is more important since it has physical significance. The value of $\sigma_{\max}$ directly influences the size of near tip plastic zone during crack growth (Tvergaard and Hutchinson, 1992; Wei and Hutchinson, 1999). With changes in the crack tip plastic flow, the plastic dissipation Γ_{p} varies and alters the total fracture energy Γ. Of the two critical fracture parameters, Γ_{o} may be estimated from fracture toughness test but estimation of $\sigma_{\max}$ is usually more difficult.

Unlike homogeneous materials where Γ_{o} and $\sigma_{\max}$ can be assumed to be *constant* throughout the media, they are not unique in graded materials. The two parameters must be defined as functions of position (e.g., $\Gamma_{\mathrm{o}}(x)$, $\sigma_{\max}(x)$) or composition of multiple phases at the a given location. Usually, graded materials are fabricated from varying composition of two phases. Suppose the fracture parameters depend solely on composition (i.e., volume fractions of two phases) and can be defined as functions of volume fraction of one phase as

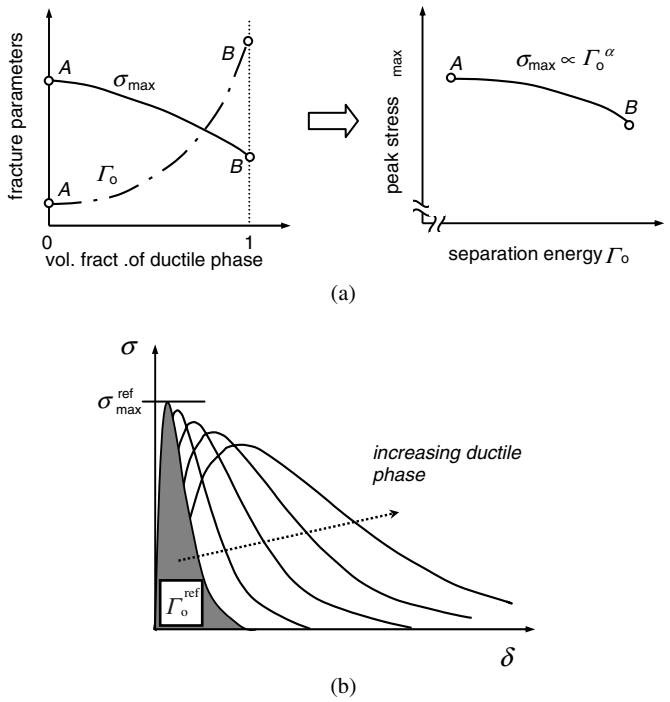

Fig. 2. (a) Schematic illustration of fracture parameters shown as function of volume fraction of ductile phase. When they are smooth and monotonic, a power-law relation between them can be assumed. (b) Traction–displacement relation as it varies within graded region. The separation energy increases while the peak stress decreases along the direction of increasing ductile phase ($\alpha < 0$).

shown in Fig. 2(a). Note such a plot may be constructed from testing several composites with same phases but with different volume fractions, although it can be extremely complex. In the figure, it is assumed that the peak stress decreases while the separation energy increases with larger ductile phase. If both functions are sufficiently smooth and monotonic, one may produce a direct relationship between Γ_o and σ_{max} as shown in the next figure. Furthermore, as a first order approximation, this relation may be expressed with a power-law equation as,

$$\frac{\sigma_{max}}{\sigma^*_{max}} = \left(\frac{\Gamma_o}{\Gamma^*_o}\right)^{\alpha}. \tag{9}$$

Here Γ^*_o and σ^*_{max} are the parameters defined at a reference point (e.g., elastic phase). The exponent α can be any real number that defines the variation of σ_{max} as a function of Γ_o. Without such an assumption, independent determination of spatial variant quantities Γ_o and σ_{max} would be difficult. With this relation, one needs to define a single material parameter α and Γ_o variation (as a function of position or composition). Introduction of the above relation should significantly reduce efforts required to obtain σ_{max} variation which is generally very difficult quantity to measure.

The exponent influences the peak stress as follows. Suppose a graded specimen with increasing Γ_o along the x-axis (e.g., graded ceramic–metal specimen). If $\alpha > 0$, then σ_{max} also increases with larger x. On the other hand, when $\alpha < 0$, lower σ_{max} prevails even though Γ_o increases with x. With $\alpha = 0$, σ_{max} is constant and independent of Γ_o. Suppose a crack propagates from the elastic phase (i.e., ceramic) to the graded elastic–plastic phase (i.e., ceramic–metal), and then it is likely to encounter a decreasing peak stress with lowering of yield stress while the separation energy increases as more energy is required in the ductile phase. To represent this condition, α must be set negative. The various σ–δ relations under Mode I condition

for the case of $\alpha < 1$ is illustrated in Fig. 2(b). At each material point, the area underneath the σ–δ curve corresponds to the local separation energy. The exact value of α should depend on the composition and the fabrication process of the graded material. It may be also influenced by loading and constraint conditions but these factors can be assumed as second order effects so that we may treat the exponent α as a material parameter.

The cohesive relation (8) is generally implemented in non-linear spring type elements (e.g., Needleman, 1987). In the present analysis, in order to use the explicit time-integration scheme, the relation is imposed in quadrilateral elements that are placed along continuum element boundaries. In order to limit the artificial influence of cohesive elements on the overall response small, their thickness h is set less than 1% of the adjacent elements' size. In addition, the initial stiffness of cohesive element (estimated from $\sigma_{\max}/h\delta_{\mathrm{o}}^{\mathrm{n}}$) are set close to that of the bulk material to avoid altering overall rigidity of the structure as well as stress wave propagation characteristics. The mass density of cohesive element is also set close to the bulk density. The accuracy of this procedure was compared and verified with known exact solutions of linear elastic models.

3. Dynamic crack growth in elastic–plastic graded material

3.1. Double cantilever beam model

To examine the dynamic failure growth characteristics of graded materials and feasibility of proposed model, a simple fracture configuration is considered. Here a double cantilever beam (DCB) specimen under dynamic load is selected. This model consists three regions, ceramic (linear elastic), graded and metal (elastic–plastic) phases, as shown in Fig. 3(a). Initially, the crack tip is located within the ceramic region at $x = 0$. This specimen is loaded suddenly at $t = 0$ with constant velocity at the opening end of the specimen as shown in the figure. The stress waves traverse to the crack tip and initiate dynamic crack growth. The graded region begins at $x = 1$ mm and spans for 5 mm. The material properties of the elastic phase are the Young's modulus $E = 350$ GPa, the Poisson's ratio $v = 0.25$, mass density $\rho = 3,900$ kg/m^3 and the separation energy per unit area $\Gamma_{\mathrm{o}} = 30$ J/m^2. These values approximate those of Al_2O_3. The elastic–plastic phase models a ductile steel with $E = 200$ GPa, $v = 0.3$, $\rho = 7,800$ kg/m^3, and $\Gamma_{\mathrm{o}} = 2000$ J/m^2. Its plastic behavior is described by the yield stress $\sigma_{\mathrm{o}} = 700$ MPa and the linear strain hardening modulus $H = 10$ GPa. Note these values were chosen rather arbitrary since our objective is to gain the qualitative insights to the crack growth in the graded region and not modeling of a particular graded material at this stage. Also due to the symmetry condition, the crack propagates under pure Mode I condition.

Within the graded region, the volume fractions of ceramic and metal phases are set to vary linearly with x. Since the composition changes with x, the material properties must also vary with location (e.g., $E = E(x)$). There are several theories to estimate effective properties of two-phase composites. Here the so-called *modified rule-of-mixture* (Suresh and Mortensen, 1998) is assumed. According to this model, the effective Young's modulus is the weighted average of the moduli for ceramic and metal. Other material properties are also determined using the modified rule-of-mixture. Fig. 4 shows the gradually varying stress–strain relationship within the FGM region. Here, the yield stress decreases with increasing metal phase.

3.2. Computational procedure

Due to the symmetry about the crack plane, only the top half of double cantilever beam configuration is modeled in the finite element analysis. The finite element mesh for half model contains about 43,000 four-noded plane strain elements and 950 cohesive elements as shown in Fig. 3(b). The cohesive elements are placed along the x-axis ($x > 0$). The element length along the crack path is set at 10 μm, which should be small enough to resolve complex near tip stress state. The separation energy Γ_{o} within the FGM region (1 mm $< x <$ 6 mm) is assumed to increase linearly with x as shown in Fig. 5(a). Using (9), the peak stress $\sigma_{\max}$ needed for the cohesive relation are

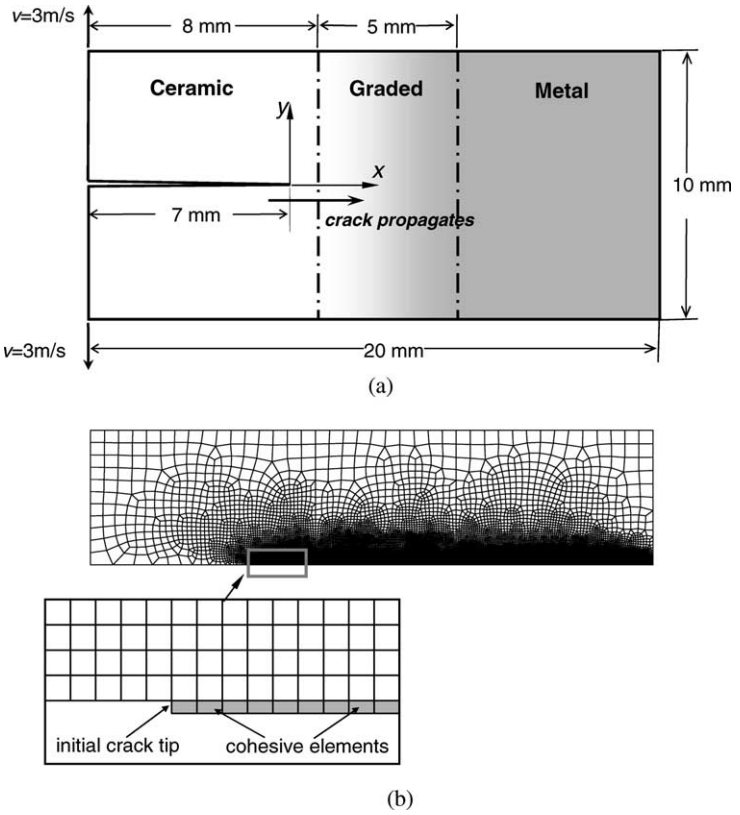

Fig. 3. Graded double cantilever beam (DCB) model under dynamic loading. (a) Schematic of the model. (b) Finite element mesh for the top half. Cohesive elements are placed along the predefined crack path.

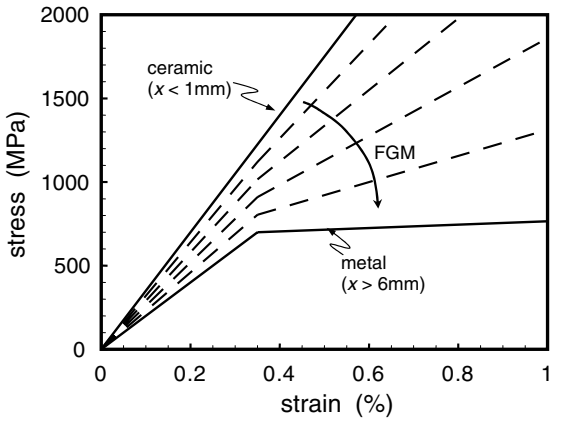

Fig. 4. Bi-linear stress–strain relations within DCB model. It varies from pure ceramic to pure metal in the graded region (1 mm $< x <$ 6 mm).

determined. In order to determine its effects, three different values of $\alpha = 0, -0.1, -0.2$ are considered. For $\alpha < 0$, the peak stress decreases as crack propagates from the elastic phase to the metal-rich elastic–plastic phase. The variation of $\sigma_{\max}$ within the graded region is shown in Fig. 5(b). For the reference parameters in (9), we have selected the corresponding values of ceramic. They are $\Gamma_{\mathrm{o}}^{*} = 30$ J/m^2 for the separation energy, and $\sigma_{\max}^{*} = 3.68$ GPa for the peak stress.

The finite element analyses are carried out with explicit time integration scheme. At $t = 0$, the specimen is loaded by a pair of constant velocity ($v = 3$ m/s) prescribed at the left edge. The time increment is typically $\Delta t = 4 \times 10^{-10}$ s. At every time increment, various parameters are monitored, including the crack tip position and energy values.

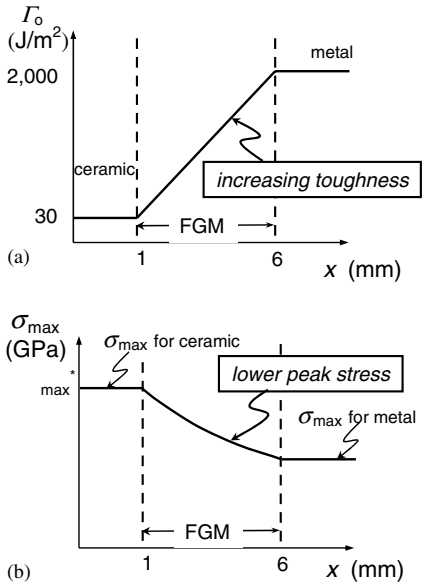

Fig. 5. Variations of cohesive parameters within FGM region for $\alpha < 0$. (a) Separation energy. (b) Peak separation stress.

3.3. Crack propagation behavior

After loading waves reach the crack tip and sufficient crack driving force builds up, crack propagation occurs at around $t = 5$ μs. The crack growth behaviors of the three cases are shown as functions of time in Fig. 6(a). Initially, the crack grows similarly in all cases while it is still within the elastic region (up to $\Delta a = 1$ mm). Afterward, the propagation behavior varies for different α's as the crack enters the graded region at around $t = 7$ μs. The crack tip speeds are determined from the time derivatives and shown in Fig. 6(b). The fastest crack is observed for $\alpha = -0.2$ as it traverses the entire FGM region in less than 19 μs to reach the metal phase (i.e., $\Delta a = 6$ mm at $t = 26$ μs). The highest crack tip speed is about 690 m/s. In the case of $\alpha = -0.1$, the propagation speed is somewhat slower than that of $a = -0.2$. The crack growth is slowest for $\alpha = 0.0$. The crack almost arrests when it enters the metal phase ($\Delta a = 6$ mm), and the slow propagation stage lasts more than 20 μs. These propagation behaviors are direct outcome of different peak stress variations since all other properties, including the separation energy,

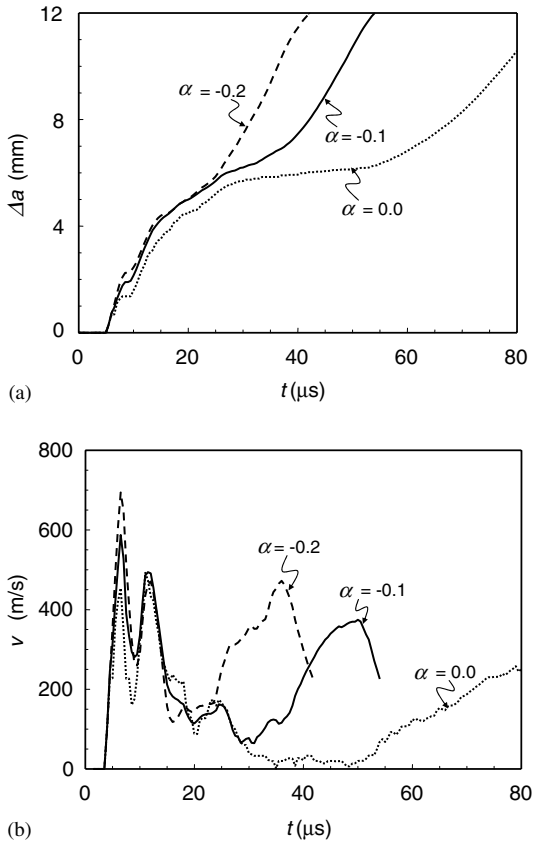

Fig. 6. Crack propagation in DCB model for different peak stress variation defined through α. The peak stresses are lowest for $\alpha = -0.2$. (a) Crack advance. (b) Crack tip speed.

are identical in the three cases. For $\alpha = 0$, -0.1, -0.2, the σ_{max} in the metal phase is 3.68, 2.42 and 1.59 GPa, respectively. When a larger σ_{max} is required to propagate, crack growth requires sufficient stress build-up and slows the crack tip speed. Within the elastic–plastic region (graded and metal phase), a larger peak stress also causes near tip plastic zone to enlarge that leads to greater energy dissipation associated with the crack growth.

According to (4), the total fracture energy during propagation is defined as the sum of the separation energy and the plastic dissipation energy. Thus, a larger plastic dissipation translates to higher crack growth resistance. In order to examine this behavior more closely, various energy values during propagation are extracted. Fig. 7(a)

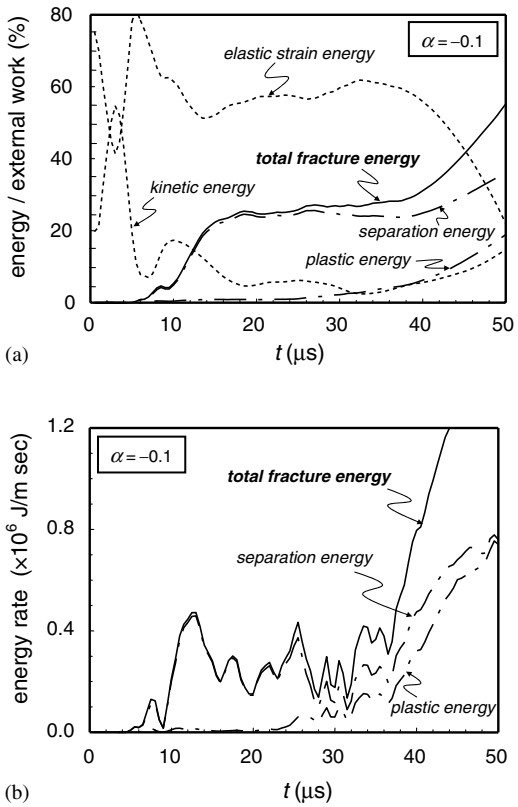

Fig. 7. (a) Evolutions of various energy components during crack propagation for $\alpha = -0.1$. Total fracture energy is the sum of separation and plastic energies. They are normalized with external work. (b) Time derivatives of energies. Elastic strain and kinetic energies are not shown for clarity.

shows the partitioned energy components during crack propagation for $\alpha = -0.1$. They are normalized by the external work due to the loading, which is equal to the sum of elastic strain energy, kinetic energy, plastic energy/dissipation and separation energy. The separation energy is obtained by integrating the potential Φ, shown in (8), of all the cohesive elements. Note that the separation energy in the figure represents the accumulation of energy consumed for separation, while Γ_o in (4) is the energy rate per unit advance of separation. Also in the figure, sum of the separation energy and the plastic dissipation is denoted as the total fracture energy since it represents the energy directly consumed by the crack growth. In this model, the plastic deformation is confined to near crack tip region and the plastic dissipation occurs only by the propagation. At the beginning, most of external work is transferred into the elastic strain and kinetic energies. At about $t = 4$ μs, the kinetic energy peaks and starts to drop relatively. As crack tip enters the graded region at $t \sim 7$ μs, the separation energy continues to increase and the plastic dissipation begins. The plastic energy remains relatively small while within the graded region (~ 7 μs $< t \lesssim 27$ μs). The plastic flow is limited since the ratio of peak stress to yield stress stays low and reaches $\sigma_{max}/\sigma_o = 3.4$ only at the end of graded region (for $\alpha = -0.1$). Once the crack enters the metal phase, the plastic deformation increases rapidly. At $t = 50$ μs, the total fracture energy accounts for 50% of the internal energy.

In order to relate the crack propagation to the balance of energy rate as discussed in Section 2.1, time derivatives of the energy quantities are calculated. At each time increment, the balance equation in (6) is satisfied within 0.1% of the external power P, which attests the accuracy of calculations. Fig. 7(b) shows the rates of the separation energy F_o and the plastic dissipation $\dot{U}_{pl}$ as well as the total fracture energy $(F_o + \dot{U}_{pl})$. The other components were not shown for clarity. Although the rate of plastic energy is low at beginning, it reaches close to the rate of separation energy when the crack enters the metal region ($t <\sim 27$ μs). These energy rates can be divided by the crack tip speed to obtain Γ_o, Γ_p and $\Gamma(= \Gamma_o + \Gamma_p)$, respectively, as shown in Fig. 8(a). It is interesting to note that while the energy rates (Fig. 7(b)) and the crack tip speed (Fig. 6(b)) are highly oscillatory, the divisions show much smoother behaviors. In the figure, the separation energy increases while the crack tip is within the grade region (~ 7 μs $< t \lesssim 27$ s), but remains constant in the metal phase. This output is consistent with the imposed separation energy variation in the graded region. Within the metal phase, the contribution from plastic dissipation increases rapidly. After $t = 30$ μs, the time variation slows down, which is an indication of steady state condition within the homogeneous metal phase.

The total fracture energy per unit advance Γ is re-plotted as function of the crack growth distance

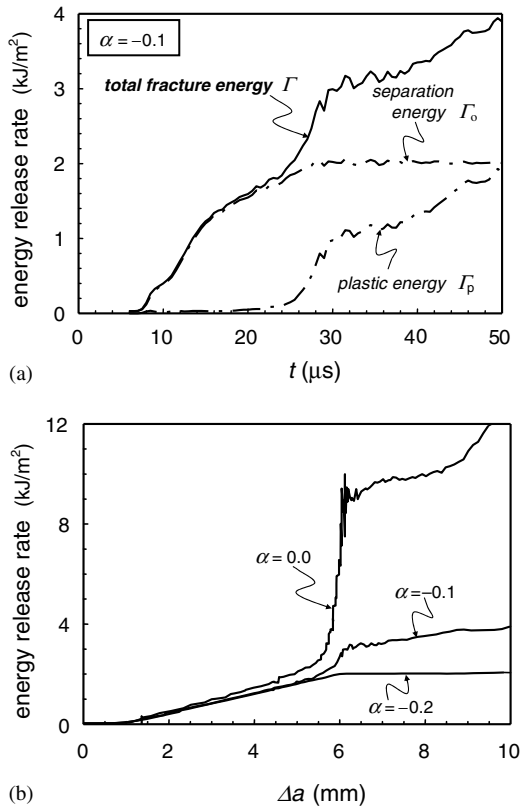

Fig. 8. (a) Energy release rate of moving crack shown as function of time for $\alpha = -0.1$. Total fracture energy is the sum of the separation and plastic energies. (b) Total fracture energy shown as function of crack growth for various α's.

in Fig. 8(b). Here the results of other α values are also shown. Physically, this exponent controls the amount of plastic dissipation as the crack propagates through the graded and metal region. For $\alpha = -0.2$ (lower peak stress σ_{max} case), the plastic dissipation during crack propagation is negligible. This means $\Gamma_p \ll \Gamma_o$ and $\Gamma \approx \Gamma_o$. In fact, the result closely follows the prescribed variation of Γ_o (i.e., linear increase from 30 to 2000 J/m^2 for 1 mm $< x <$ 6 mm and constant for $x >$ 6 mm at 2000 J/m^2). On the other hand, for $\alpha = 0$, the extent of plastic deformation is much greater (with higher peak stress σ_{max}). Here, the plastic dissipation accounts as much as 80% of the total fracture energy. Intermediate results can be observed for $\alpha = -0.1$ where the magnitudes of Γ_o and Γ_p are about the same near the end. To verify the accuracy of computed Γ_o, a separate model without any plastic deformation ($\Gamma_p = 0$) is constructed and the domain integral (2) is used to compute Γ. The integral Γ is always within 1–2% of Γ obtained from the balance of energy rate equation.

As noted earlier, Γ_o and σ_{max} are the critical parameters to simulate crack propagation. The assumed relation proposed in (9) significantly reduces the task of defining Γ_o and σ_{max} individually since the exponent α defines σ_{max} variation with that of Γ_o. In the DCB model, the crack propagation behavior is very sensitive to the value of α since it directly controls the peak stress and the amount of plastic dissipation. A suitable value of α for a given graded material must be obtained from experimental investigations.

4. Multiple crack growths in graded layer

4.1. Impact load model

The computational procedure described for the graded fracture specimen is extended to crack a more complex dynamic failure analysis. Here a FGM model subjected to a high velocity rod impact is considered. Unlike the previous model with well-defined crack path, the impact generates multiple crack nucleations at arbitrary locations and growths along arbitrary directions. The impact load model consisting of a protective FGM layer and a metal substrate is shown in Fig. 9(a). This is a simplified model and not meant to simulate actual projectile striking or penetration phenomena. However, the model is still sufficient to verify applicability of the current simulation procedure in complex loading environments.

In order to minimize lateral boundary effects, the width of bi-layer structure is chosen to be much larger than its thickness. Within the protective layer, the material is graded along the vertical direction with the top surface being pure ceramic and at the interface being metal. The material properties are chosen to be same as those used for the DCB model. For the ceramic phase, they are $E = 350$ GPa, $\nu = 0.25$, $\rho = 3900$ kg/m^3 and $\Gamma_o = 30$ J/m^2. For the metal phase, they are

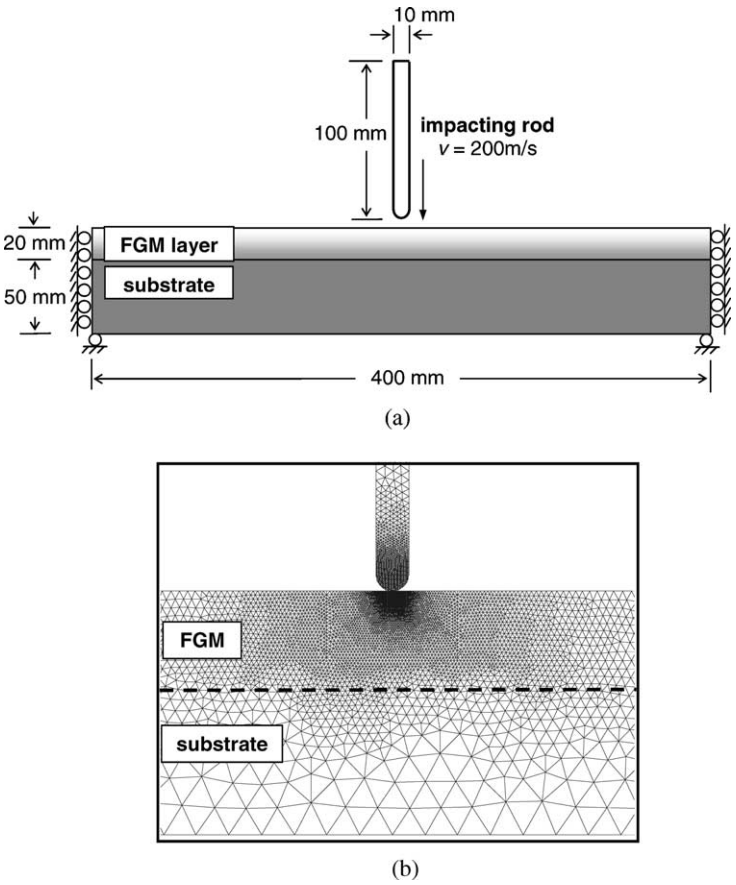

Fig. 9. (a) Schematic of protective FGM layer and substrate subjected to impacting rod. (b) Finite element mesh near the impact. Cohesive elements are distributed within FGM underneath the impact.

$E = 200$ GPa, $v = 0.3$, $\sigma_o = 700$ MPa, $H = 10$ GPa, $\rho = 7800$ kg/m^3 and $\Gamma_o = 2000$ J/m^2. Initially, the grading is assumed to be linear and the same property variations are assumed in the graded layer. In addition, the rod and the substrate are treated as elastic material with E, v and ρ of the metal. For the fracture parameters, the power exponent of $\alpha = -0.1$ and the reference values of $\Gamma_o^* = 30$ J/m^2 and $\sigma_{max}^* = 3.68$ GPa are chosen in (9).

4.2. Computational procedure

Instead of using four-noded quadrilateral elements as in the DCB analysis, three-noded constant strain triangular elements are utilized in the construction of mesh. This choice allows greater flexibility in propagation paths and directions than those with four-noded elements. In addition, more stable numerical convergence is obtained with the triangular elements. Note that the propagation paths are still restricted along the element boundaries and there is some degree of mesh-dependence. About 15,000 plane strain elements are used to construct the model shown in Fig. 9(b). Near the impact region, small elements with length of 100 μm are placed and the element sizes are gradually increased away from the impact location. To simulate crack propagations, approximately 10,500 cohesive elements are distributed along the element boundaries within a rectangular region underneath the rod impact (20 mm × 30

mm). This region spans the thickness of graded layer. They are not distributed over the entire model to reduce computational time. Unlike the DCB model under Mode I condition, cracks are expected to propagate under mixed-mode condition. Initially the ratio of Mode II to Mode I separation energies is set unity ($q = 1$) in (8), and the separation stress of Mode II, is set to be same as that of Mode I (i.e., $\tau_{\max} = \sigma_{\max}$). At $t = 0$, initial velocity of 200 m/s is prescribed for the metal rod. The contact condition is imposed between the rod and the top surface of the FGM layer to simulate the indentation by the rod. All computations are carried as finite deformation analyses.

In any dynamic simulations, stability of calculation is an important consideration. Here, it is influenced by various factors such as element sizes/shapes and the traction–separation law of cohesive elements. Instability is more prevalent when primary loading condition is compression rather than tensile. Compressive load not only initiates complex fracturing modes but also tends to overlap elements. In order to improve the numerical stability, a small damping is artificially introduced in this calculation. Various tests indicate some influence of damping with its effects to be 2–5% in terms of energy calculations. To further ensure the accuracy of explicit calculations, a time increment is set very small at about 2×10^{-11} s. Each impact analysis requires about half a million increments for up to 8 μs calculations.

4.3. Multiple crack initiations and growths

At $t = 0$, the rod strikes the FGM layer at 200 m/s (about 2% of the ceramic bar wave speed). Initial fracture occurs immediately after the impact. Essentially the rod crushes and breaks apart the material underneath the contact. In fact almost all the element boundaries are separated eventually within this region. These fracturing primary occur under Mode II condition. Subsequently, some of them radiate outward. A sequence of cracking is illustrated in Fig. 10. Crack propagation directions can be classified into types. One tends to propagate horizontally and the other tends to propagate downward. The former type has greater Mode I component as can be observed from wider surface separations, while the latter type is generally Mode II dominant. These cracks have no or very small normal separations since compression keeps two surfaces in contact. But intense shear causes relative sliding to cause Mode II fracture. At $t = 8$ μs, the separation energy released by all the cracks totals 400 J/m, of which about 70% of the energy release is by pure or nearly Mode II cracks. This is an indication of dominant Mode II fracture condition. Crack propagation speeds vary for different cracks but some reach up to 500 m/s. In general, horizontal cracks grow faster than those along the vertical direction. Since the deeper regions are more resistant to crack propagation (with larger Γ_o), it is harder for cracks to propagate through. The figure also illustrates complete separation of several fragments adjacent to the impact. Their sizes range from a single element size (~100 μm) to about 3 mm. Note that mesh is generated asymmetrically across the center vertical line to avoid symmetrical crack profile. As discussed earlier, the cracking pattern is mesh-dependent since they can only occur along element boundaries. The effects of mesh-dependence are discussed in Section 4.5.

The state of stresses after impact is shown in Fig. 11, where shades of effective stress (σ_e) and pressure ($-\sigma_h$) at $t = 8$ μs are illustrated. In the FGM layer, largest effective stress (>8 GPa) is observed directly underneath the impact. In the pressure contours, largest compression is observed along the contact surface. In both figures, unlike a regular model without cracks, the shades are not continuous. This is the outcome of multiple fracturing, which generates very complex stress state. At $t = 8$ μs, the total energy transferred into the layer and the substrate is about 20% of the initial kinetic energy of the rod. The tip velocity of rod is still about 120 m/s. This means the impact will continue. However excessive element distortions occur within the high-pressured region and cause numerical instability. Since re-meshing is not possible or practical with cohesive elements, the computation is terminated at this point. The simulation of penetration can be carried out with other means of failure criteria, such as one based on the maximum plastic strain (Rajendran, 1998),

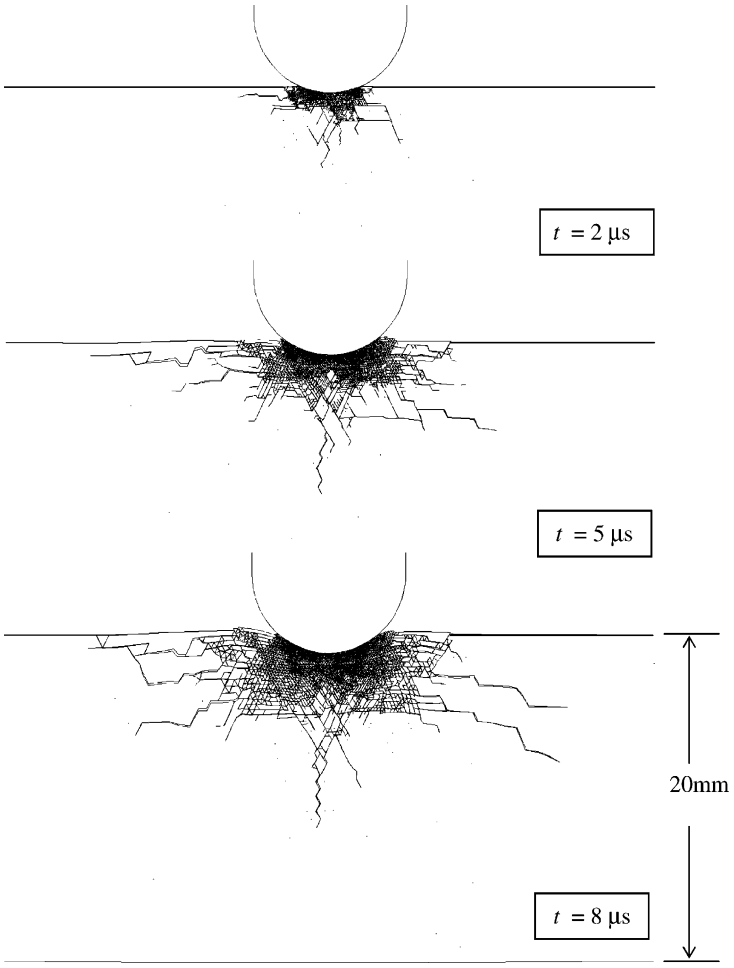

Fig. 10. Profiles showing sequence of crack initiations and growths after impact.

although such a model would not be applicable with models containing a brittle phase.

4.4. Effects of material gradation

In the initial model, the material composition within the graded layer is assumed to vary linear with the depth. However, in real applications, the gradation can be varied to achieve optimal effects, which is the strength of FGMs (Chin, 1999). Here, we investigate the effects of material gradation on the fracture behaviors. The geometry, loading conditions and material properties of ceramic and metal are kept the same while different compositional gradations are prescribed. To describe the gradation conveniently, the variation of material composition is set to follow the power-law relation as,

$$V_{\mathrm{m}} = (z/d)^n. \tag{10}$$

Here, V_{m} is the volume fraction of metal phase, z is the distance measured from the top surface, d is the thickness of the FGM layer ($d = 20$ mm), and n is the material gradation parameter. The metal volume fraction is always $V_{\mathrm{m}} = 0$ at $z = 0$, and $V_{\mathrm{m}} = 1$ at $z = d$. If $n = 1$, the material composition varies linearly, as that is the case of the initial

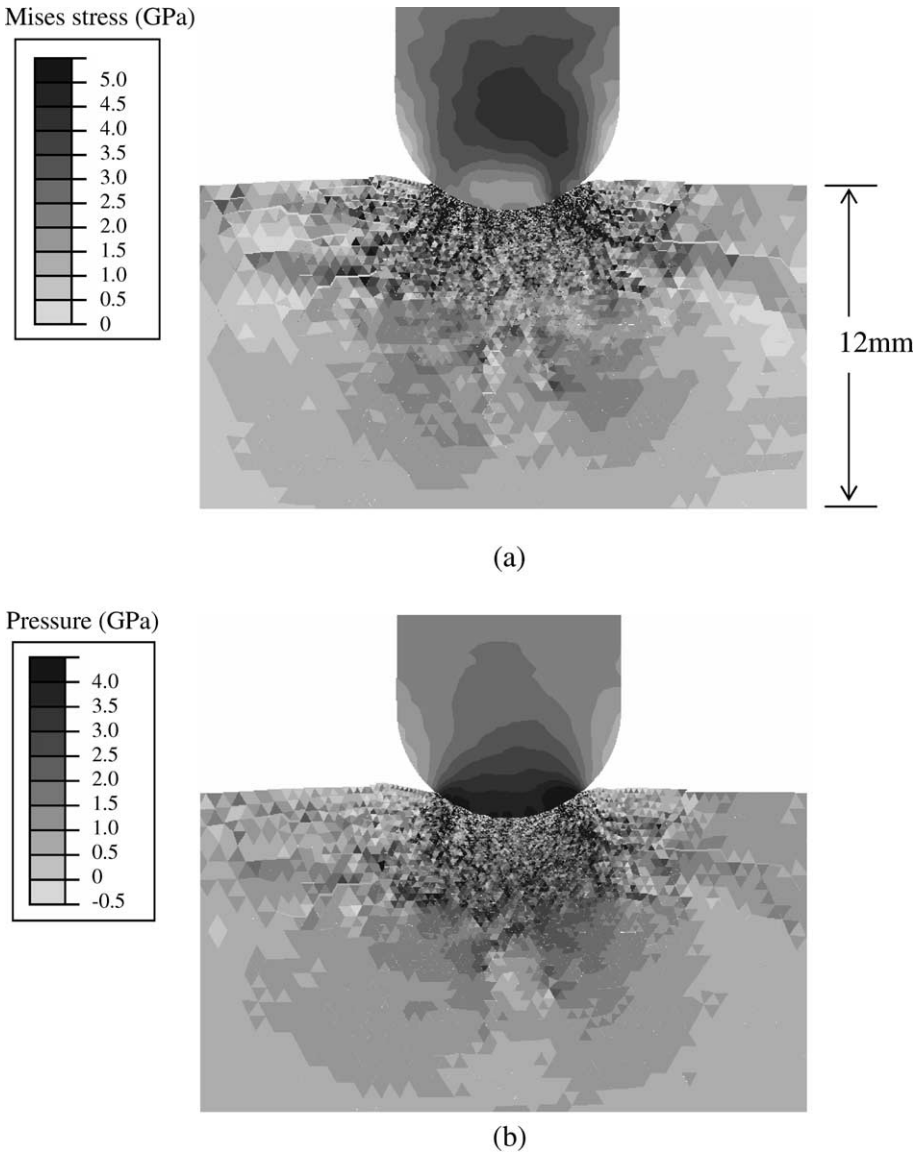

Fig. 11. Shades of stresses at $t = 8$ μs after impact shown for (a) effective stress (σ_e), and (b) pressure ($-\sigma_h$). Discontinuous stresses are due to cracking.

analysis. Here additional cases for $n = 1/3$ and 3 are considered. Also, pure ceramic case, corresponding to $n \to \infty$ is also examined. The gradations according to the power-law for $n = 1/3$, 1, 3 and ∞ are illustrated in Fig. 12.

The profiles of cracks at $t = 8$ μs for $n = 1/3$, 1, 3 and ∞ are shown in Fig. 13. It is observed that for larger n (i.e., more ceramic phase), cracks tend to propagate farther downward. At $t = 8$ μs, a crack tip reaches the bottom of graded layer (i.e., the interface with substrate) for the pure ceramic case ($n \to \infty$), while cracks extend only mid-way through the thickness for $n = 1/3$ case. These behaviors are dictated by the imposed toughness variations through-thickness. It is more difficult for cracks to propagate where the volume fraction

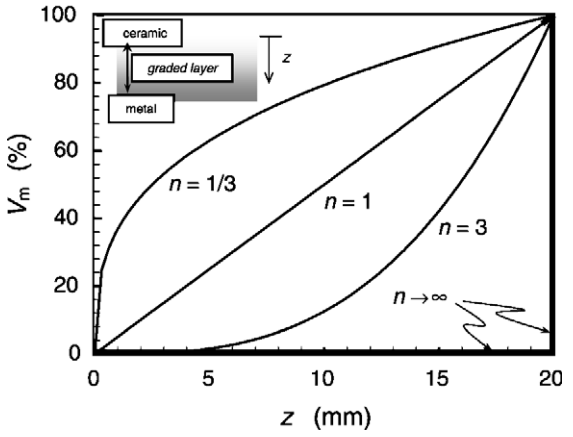

Fig. 12. Various grading styles shown with through-thickness change of metal volume fraction. Variations based on power-law form are assumed. Note $n \to \infty$ corresponds to pure ceramic layer (i.e., $V_m = 0$ for all z).

of metal phase is larger. For horizontal cracks, the extensions are similar in all the cases.

The effects of gradation on energy components are also examined. The partitioned energy within the FGM layer normalized by the initial kinetic energy of the rod (impact energy) is shown for various cases in Fig. 14. Here, the separation energy is obtained by summing the products of every cracked element length and its consumed energy Φ. In the figure, the total dissipation is the sum of the separation energy and the plastic energy/dissipation. Note that unlike the DCB model, the plastic energy includes significant plastic flow directly caused at the impact. In all cases, the time variations of recoverable energies (elastic strain energy and kinetic energy) are very similar regardless of gradation. On the other hand, the dissipative energies are highly influenced by various gradations. The models with smaller n (i.e., greater metal content) show larger plastic energy as well as larger separation energy. The latter fact does not suggest there are more cracks but each crack has greater separation energy Γ_o. For the case of

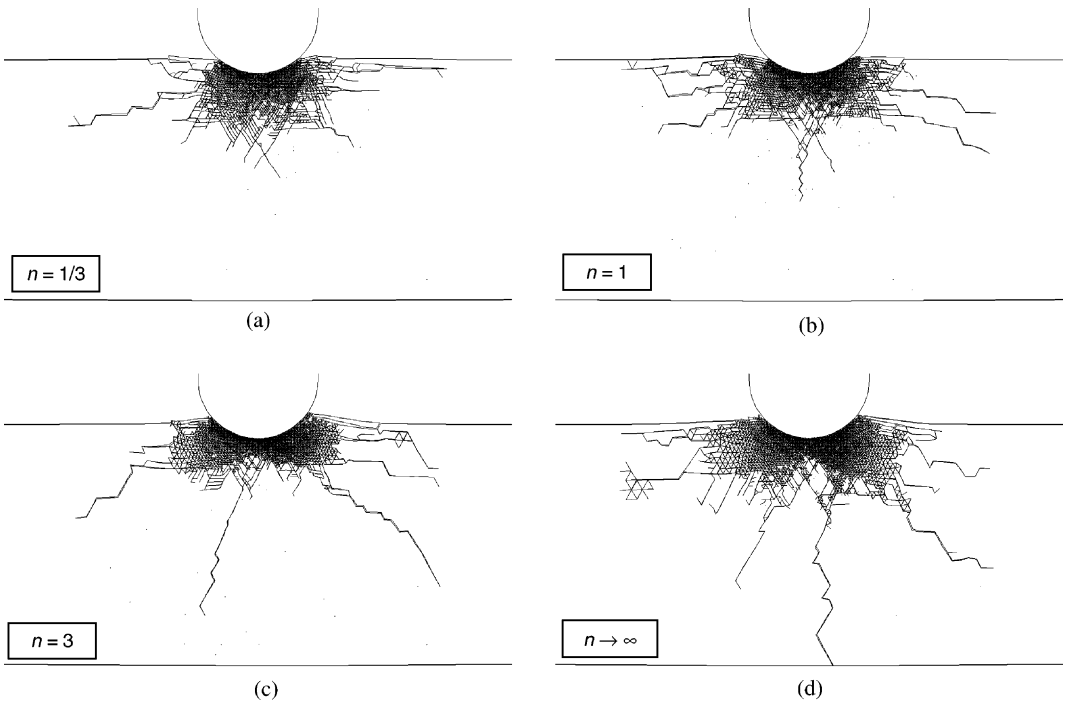

Fig. 13. Crack profiles at $t = 8$ μs for different gradations; (a) $n = 1/3$, (b) $n = 1$, (c) $n = 3$, and (d) pure ceramic ($n \to \infty$). Greater vertical cracks are observed with larger n.

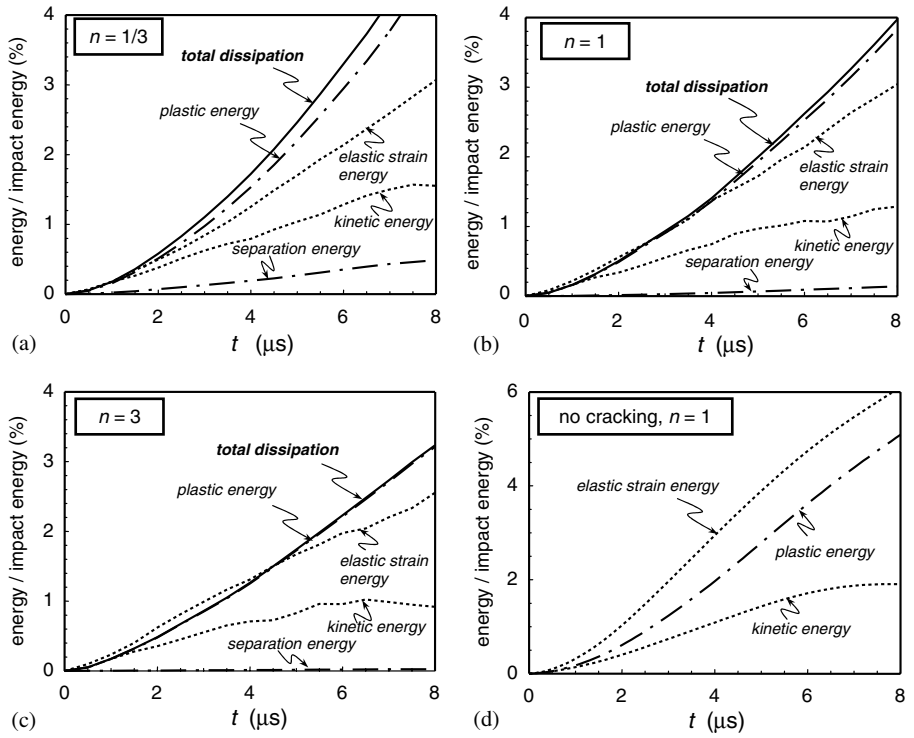

Fig. 14. Evolutions of various energy components in the FGM layer shown for various gradations: (a) $n = 1/3$, (b) $n = 1$, (c) $n = 3$. Total dissipation is the sum of separation and plastic energies. (d) For reference, no cracking model with $n = 1$ is shown.

$n = 1/3$, the total dissipated energy reaches more than 5% of the impact energy at $t = 8$ μs.

In order to quantify the effects of cracking more clearly, a separation calculation is carried out without cracks (i.e., no cohesive elements) for $n = 1$ gradation. Its energy components are shown in Fig. 14(d). In comparison with the model that allows cracking (Fig. 14(b)), the elastic strain and kinetic energies are far greater (nearly double of those without cracks at $t = 8$ μs). More importantly, the plastic energy also exceeds the model with cracks by about 25%. They are the outcome of stiffer response without cracks. The comparison study elucidates that the presence of cracking has a significant effect in the energy absorption characteristics. Although cracks only account for small energy absorption (separation energy is 0.14% of impact energy at $t = 8$ μs as shown in Fig. 13(b)), their presence causes other energy components to change more significantly. Physically, the cracking alters the effective modulus and the energy transfer mechanisms to the layer.

4.5. Effects of mode dependency

In the previous calculations, the separation energy under pure Modes I and II conditions are assumed to be equivalent (i.e., $q = 1$). In many materials, it is known that the toughness under Modes I and II is not the same. Here we investigate the mode dependency by prescribing greater separation energy under Mode II condition. In the calculations, all the parameters are kept the same but the mode dependent parameter is set as $q = 1.8$ (i.e., 80% more energy under Mode II condition). The gradation is assumed to be linear ($n = 1$).

With larger q, less cracking occurs within the same time period. Fig. 15(a) shows the crack profile at $t = 8$ μs. Comparing with $q = 1$ shown in Fig. 13(b), the extent of cracking is confined and

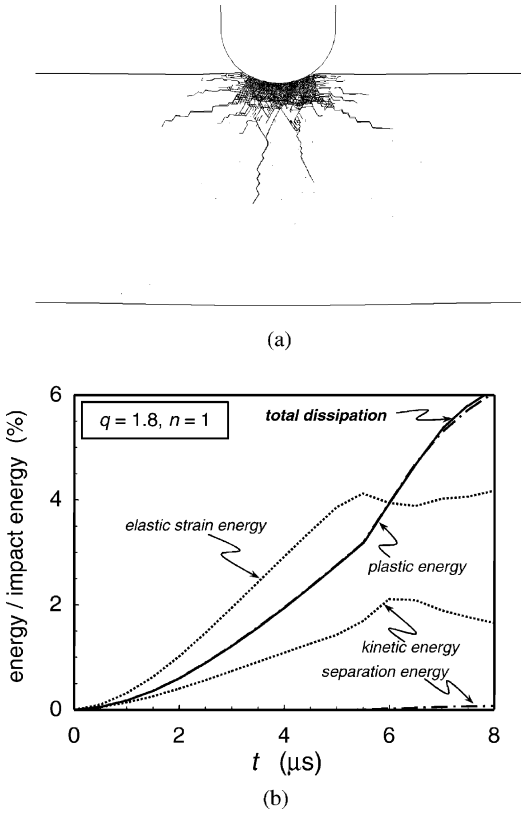

Fig. 15. Effects of larger Mode II toughness ($q = 1.8$). (a) Crack profile at $t = 8$ μs. (b) Evolutions of energy components. Linear grading is assumed ($n = 1$).

there are significantly less cracks near the free surface. In fact, initial cracking occurs at a later time and there are less Mode II cracks. The energy components in the FGM layer are also shown in Fig. 15(b). Here up to $t \sim 5.5$ μs, the behaviors of elastic strain, kinetic and plastic energies are identical to those for the no-crack model shown in Fig. 14(d). At about $t = 5.5$ μs, crack nucleation and growth suddenly take place, as indicated by sudden changes in the curves. Beyond this time, the strain energy and kinetic energy essentially cease to increase while the plastic energy rises more rapidly. This is probably due to large plastic flow caused by crack propagations (i.e., near-tip plasticity). The difference between the plastic energy curves in Figs. 14(d) and 15(b) can be attributed to the plastic flow solely from the crack propagations. The amount of plastic energy at $t = 8$ μs is 50% and 20% higher than those for the $q = 1$ and no-crack cases, respectively (Fig. 14(b) and (d)). In summary, a larger q slows crack initiations, but once they begin, the propagations are accompanied by larger plastic flow. This result further confirms that cracks have significant influences on energy absorption characteristics although separation energy its may be small.

For purpose of protecting the substrate, it is desirable to have the layer dissipate as much energy as possible. Based on the current analysis, albeit with a simplified model and limited computations, it appears the separation energy due cracking account for a small part of the total dissipative energy. However, the cracks play far more important role since their presence significantly influences the behaviors of other energy components. Thus, accurate crack models are essential in obtaining the energy absorption behavior. In real applications, the design of material gradation may require additional factors such as weight, thermal barrier property, stress concentration in the substrate and long dwell time of projectile (Chin, 1999). The current analysis only elucidates a few basic relationships among gradation, cracking patterns and energy absorption. Additional work is necessary to clarify other important factors, including the strain rate dependency and the crack tip speed.

4.6. Effects of mesh-dependence

In many crack propagations with finite element analysis, mesh-dependency is difficult to avoid. In order to quantify such an effect, we generate a separate mesh with larger element sizes. Here, the element lengths are set twice as large (4 times as large in area) as the previous case. The case of linear gradation ($n = 1$) and no mode-dependency ($q = 1$) are considered, and all other quantities are kept the same as before. The cracking pattern for this case is shown in Fig. 16(a), which can be compared with Fig. 13(b). Although there are less long cracks, the qualitative nature of crack profile is similar to those with the finer mesh. The energy components are also computed and shown in Fig. 16(b). The general trends are very similar, and the

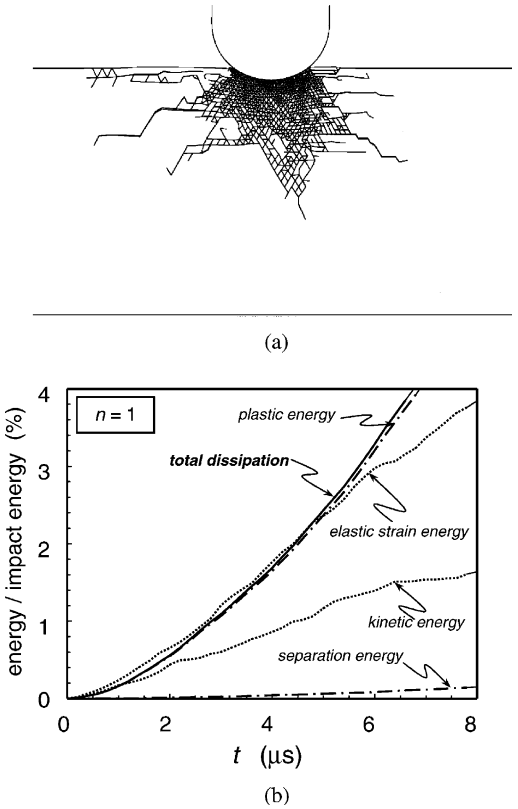

Fig. 16. Effects of mesh-dependence ($n = 1$ and $q = 1$). Elements' lengths near impact are twice as long as the initial mesh. (a) Crack profile at $t = 8$ μs, which may be compared with Fig. 13(b). (b) Evolutions of energy components, which may be compared with Fig. 14(b).

separation energy is almost identical in both meshes. The values of other energy components are about 25% higher in the coarse mesh than those in the fine mesh shown in Fig. 14(b). Physically, they represent a stiffer response since less cracking is possible in the coarse mesh. In summary, the mesh-dependence exists but these deviations are not excessive when the areas of elements are 400% larger in the coarse mesh.

5. Conclusions

Unlike homogenous materials, crack propagation in graded media is controlled by spatially variable properties. This makes its behavior to different from that of homogeneous materials. In the present study, a new criterion and procedure suitable for elastic–plastic graded materials are proposed and dynamic failure simulations are carried out. Similar approaches may be extended for other complex materials (e.g., heterogeneous materials). This is an initial study, and precise verification of the model probably requires additional studies and refinements. Meaningful experiments of actual elastic–plastic FGMs also require complex set up, including specimen fabrication, preparation and measurements. In addition, accurate simulation results are mostly likely to interpret data. Since detailed experiments of elastic–plastic graded materials are yet to be carried out, the present procedure may be applied to a simpler case of linear elastic FGMs (e.g., Marur and Tippur, 2000).

In the procedure, it is assumed that propagation is controlled by the energy and the stress required to separate surfaces. The total energy for fracture is the sum of separation energy and plastic dissipation associated with the crack growth. This idea follows from earlier crack propagation studies for homogeneous solids. For graded materials, these critical parameters are not uniform but vary over spatial coordinates. It is also assumed that a specific relationship to exist between the separation energy Γ_o and the peak stress σ_{max}. Determination of σ_{max} in any materials is difficult, and even more so for graded materials. In order to alleviate the difficulty, a power-law relationship between Γ_o and σ_{max} is assumed. Here, the power-law exponent α is treated as a material parameter which sets variation of σ_{max} for given variation of Γ_o.

The proposed simulation procedure is implemented in the DCB model where dynamic crack propagation is simulated. The model consists brittle ceramic, graded and ductile metal phases. Within the graded region, each material property is gradually varied. Our study finds results to be very sensitive to the variation of σ_{max} (specified through α). It influences the crack tip speed as well as the amount of plastic flow near the crack tip. Physically, variations of Γ_o and σ_{max} dictate how crack propagates, including its speed and fracture energy dissipations. The evolutions of various energy components are also presented and they

should be useful in understanding the fracture behavior. The total fracture energy increases as the crack enters the graded region with more ductile phase. The energy release rate is also computed from the overall balance of energy rate, and verified with the imposed variation of separation energy in the graded material.

The failure analysis procedure is also extended to a more complex geometry where rod impacts onto a graded layer bonded to a substrate. Here graded layer is designed to acts as an energy absorbing protective component. The present procedure is tested for multiple crack nucleation and growths under large compressive load. First, the analysis proves the effectiveness of present procedure for multiple crack problems. Second, the investigation on different material gradations *clearly* demonstrates their effects on cracking patterns and various evolutions of energy components. Though their quantitative accuracy may need improvement due to he simplification of model, the qualitative nature of fracture behavior is explicit. It confirms that the composition profile or gradation can be optimized to engineer improved protective layers. For an example, a gradation may be designed so that more cracks propagate along the horizontal directions to preserve the substrate yet to maximize energy dissipation in the FGM layer.

The current analysis is also carried out to study the effects of mode-dependency on the crack initiations and propagations. With larger Mode II toughness, the initiations are delayed and the evolutions of energy components are different. Some effects of mesh-dependency are also reported based on the results of a separate mesh. In all cases, the energy directly consumed by crack formations represent a small fraction of overall energy. However, the existence of cracks significantly alters the evolutions of other energy components (e.g., plastic dissipation), which suggests the importance of modeling cracks to characterize impact response.

Acknowledgements

The authors gratefully acknowledge the Army Research Office for their support under DAAD19-99-1-0318, and Professor Raman P. Singh for his assistances and discussions. The finite element analysis was carried out with I-DEAS and ABAQUS, which were available under academic license.

References

Becker, T.L., Cannon, R.M., Ritchie, R.O., 2002. Statistical fracture modeling: crack path and fracture with application to homogeneous and functionally graded materials. Eng. Fract. Mech. 69, 1521–1555.

Beltz, G.E., Rice, J.R., Shih, C.F., Xia, L., 1996. A self-consistent model for cleavage in the presence of plastic flow. Acta Mater. 44, 3943–3954.

Breitenfeld, M.S., Geubelle, P.H., 1998. Numerical analysis of dynamic debonding under 2D in-plane and 3D loading. Int. J. Fract. 93, 13–38.

Cai, H., Bao, G., 1998. Crack bridging in functionally graded coatings. Int. J. Solids Struct. 5, 701–717.

Camacho, G.T., Ortiz, M., 1996. Computational modeling of impact damage in brittle materials. Int. J. Solids Struct. 33, 2899–2938.

Chin, E., 1999. Army focused research team on functionally graded armor composites. Mater. Sci. Eng. 259, 155–161.

Gao, H., Klein, P., 1998. Numerical simulation of crack growth in an isotropic solid with randomized internal cohesive bonds. J. Mech. Phys. Solids 46, 187–218.

Geubelle, P.H., Baylor, J.S., 1998. Impact-induced delamination of composites: a 2D simulation. Composites Part B 29B, 589–602.

Hutchinson, J.W., Evans, A.G., 2000. Mechanics of materials: top-down approaches to fracture. Acta Mater. 48, 125–135.

Jin, Z., Batra, R., 1996. Some basic fracture mechanics concepts in functionally graded materials. J. Mech. Phys. Solids 44, 1221–1235.

Klein, P., Gao, H., 1998. Crack nucleation and growth as strain localization in a virtual-bond continuum. Eng. Fract. Mech. 61, 21–48.

Kolednik, O., Suresh, S., 1999. The influence of the yield strength gradient on the fracture resistance in FGMs. Functionally Graded Materials 1998. Trans Tech Publications. pp. 308–311.

Konda, N., Erdogan, F., 1994. Mixed mode crack problem in a nonhomogeneous elastic medium. Eng. Fract. Mech. 47, 533–545.

Li, H., Lambros, J., Cheeseman, B.A., Santare, M.H., 2000. Experiment investigation of the quasi-static fracture of functionally graded materials. Int. J. Solids Struct. 37, 3715–3732.

Marur, P.R., Tippur, H.V., 2000. Dynamic response of bimaterial and graded interface cracks under impact loading. Int. J. Fract. 103, 95–109.

Nakamura, T., Wang, Z., 2001. Computational simulations of crack propagation in porous materials. J. Appl. Mech. 68, 242–251.

Nakamura, T., Shih, C.F., Freund, L.B., 1986. Analysis of a dynamically loaded three-point-bend ductile fracture specimen. Eng. Fract. Mech. 25, 323–339.

Needleman, A., 1987. A continuum model for void nucleation by inclusion debonding. J. Appl. Mech. 54, 525–531.

Parameswaran, V., Shukla, A., 1998. Dynamic fracture of a functionally gradient material having discrete property variation. J. Mater. Sci. 33, 3303–3311.

Rajendran, A.M., 1998. Penetration of tungsten alloy into shallow-cavity steel target. Int. J. Impact Eng. 21, 451–460.

Repetto, E.A., Radovitzky, R., Ortiz, M., 2000. Finite element simulation of dynamic fracture and fragmentation of glass rods. Comput. Meth. Appl. Mech. Eng. 183, 3–14.

Rousseau, C.E., Tippur, H.V., 2001. Influence of elastic gradient profiles on dynamically loaded functionally graded materials: cracks along the gradient. Int. J. Solids Struct. 38, 7839–7856.

Rousseau, C.E., Tippur, H.V., 2002. Evaluation of crack tip fields and stress intensity factors in functionally graded materials: cracks parallel to elastic gradient. Int. J. Fract. 114, 87–111.

Ruiz, G., Pandolfi, A., Ortiz, M., 2001. Three-dimensional cohesive modeling of dynamic mixed-mode fracture. Int. J. Num. Meth. Eng. 52, 97–120.

Suo, Z., Shih, C.F., Varias, A.G., 1993. A theory of cleavage cracking in the presence of plastic flow. Acta Met. 41, 1551–1557.

Suresh, S., 2001. Graded materials for resistance to contact deformation and damage. Science 292, 2447–2451.

Suresh, S., Mortensen, A., 1998. Fundamentals of functionally graded materials. IOC Communications Ltd., London.

Tvergaard, V., 2001. Crack growth predictions by cohesive zone model for ductile fracture. J. Mech. Phys. Solids 49, 2191–2207.

Tvergaard, V., Hutchinson, J.W., 1992. The relation between crack growth resistance and fracture process parameters in elastic–plastic solids. J. Mech. Phys. Solids 40, 1377–1397.

Tvergaard, V., Hutchinson, J.W., 1996. Effect of strain-dependent cohesive zone model on predictions of crack growth resistance. Int. J. Solids Struct. 33, 3297–3308.

Wei, Y., Hutchinson, J.W., 1999. Models of interface separation accompanied by plastic dissipation at multiple scales. Int. J. Fract. 95, 1–17.

Xia, L., Shih, C.F., 1995. Ductile crack growth. I: A numerical study using computational cell with explicit length scales. J. Mech. Phys. Solids 43, 233–259.

Xu, X.P., Needleman, A., 1994. Numerical simulations of fast crack growth in brittle solids. J. Mech. Phys. Solids 42, 1397–1434.

Zhai, J., Zhou, M., 2000. Finite element analysis of micromechanical failure modes in a heterogeneous ceramic material system. Int. J. Fract. 101, 161–180.